

Van der Waals Multiferroic Tunnel Junctions

Yurong Su, Xinlu Li, Meng Zhu, Jia Zhang,* Long You,* and Evgeny Y. Tsymbal*

Cite This: *Nano Lett.* 2021, 21, 175–181

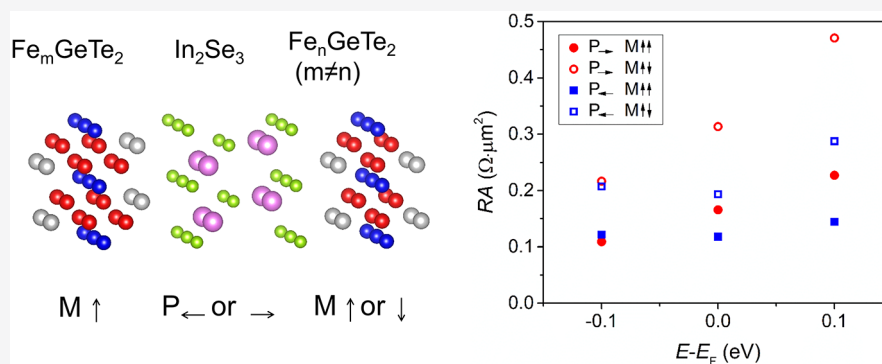
Read Online

ACCESS |

Metrics & More

Article Recommendations

Supporting Information



ABSTRACT: Multiferroic tunnel junctions (MFTJs) have aroused significant interest due to their functional properties useful for nonvolatile memory devices. So far, however, all of the existing MFTJs have been based on perovskite-oxide heterostructures limited by a relatively high resistance-area (RA) product unfavorable for practical applications. Here, using first-principles calculations, we explore spin-dependent transport properties of van der Waals (vdW) MFTJs which consist of two-dimensional (2D) ferromagnetic Fe_nGeTe_2 ($n = 3, 4, 5$) electrodes and 2D ferroelectric In_2Se_3 barrier layers. We demonstrate that such $\text{Fe}_m\text{GeTe}_2/\text{In}_2\text{Se}_3/\text{Fe}_n\text{GeTe}_2$ ($m, n = 3, 4, 5; m \neq n$) MFTJs exhibit multiple nonvolatile resistance states associated with different polarization orientation of the ferroelectric In_2Se_3 layer and magnetization alignment of the two ferromagnetic Fe_nGeTe_2 layers. We find a remarkably low RA product (less than $1 \Omega \cdot \mu\text{m}^2$) which makes the proposed vdW MFTJs superior to the conventional MFTJs in terms of their promise for nonvolatile memory applications.

KEYWORDS: Multiferroic tunnel junctions, van der Waals materials, tunneling electroresistance, tunneling magnetoresistance, multiple nonvolatile resistance states, resistance-area product

A promising spintronic device based on electron tunneling is the magnetic tunnel junction (MTJ),¹ which serves as the key building block in nonvolatile magnetic random access memories (MRAMs). Changing the magnetic alignment of two ferromagnetic electrodes in an MTJ from parallel to antiparallel causes a sizable change in tunneling resistance of an MTJ, which is known as the tunneling magnetoresistance (TMR) effect.² Functional properties of tunnel junctions can also be enhanced using a ferroelectric barrier.³ Reversal of the electric polarization of the barrier in a ferroelectric tunnel junction (FTJ) by an applied electric field produces a sizable change in resistance of the junction, that is, the phenomenon known as the tunneling electroresistance (TER) effect.^{4,5}

A multiferroic tunnel junction (MFTJ) is a FTJ with ferromagnetic electrodes or equivalently a MTJ with a ferroelectric barrier.⁶ In a MFTJ, the TER and TMR effects coexist which makes them interesting both from the fundamental point of view as well as from the point of nonvolatile low-power memory device application.^{7–9} So far, all of the considered MFTJs have been based on oxide-perovskite materials which can be epitaxially grown using

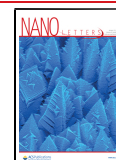
modern thin-film deposition techniques.^{10–15} However, the resistance-area (RA) product of the conventional MFTJs is typically rather large, ranging from $\text{k}\Omega \cdot \mu\text{m}^2$ ^{10,11} to $\text{M}\Omega \cdot \mu\text{m}^2$,^{12–15} which limits their application in practical devices. For instance, for a recording density of around $200 \text{ Gbit}/\text{in}^2$, an RA product of an MTJ read head should lie below $1 \Omega \cdot \mu\text{m}^2$.¹⁶ Similarly, in high-density MRAMs of about $5 \text{ Gbit}/\text{in}^2$ the impedance matching condition requires an MTJ cell to have an RA product of less than $6 \Omega \cdot \mu\text{m}^2$.¹⁷

The issue of a large RA product for conventional MFTJs mainly stems from the intrinsic properties of ferroelectric materials which has a critical thickness of about few nanometers and a relatively large energy bandgap of about several electron-volts (eV). This critical problem, impeding

Received: August 26, 2020

Revised: November 26, 2020

Published: December 2, 2020



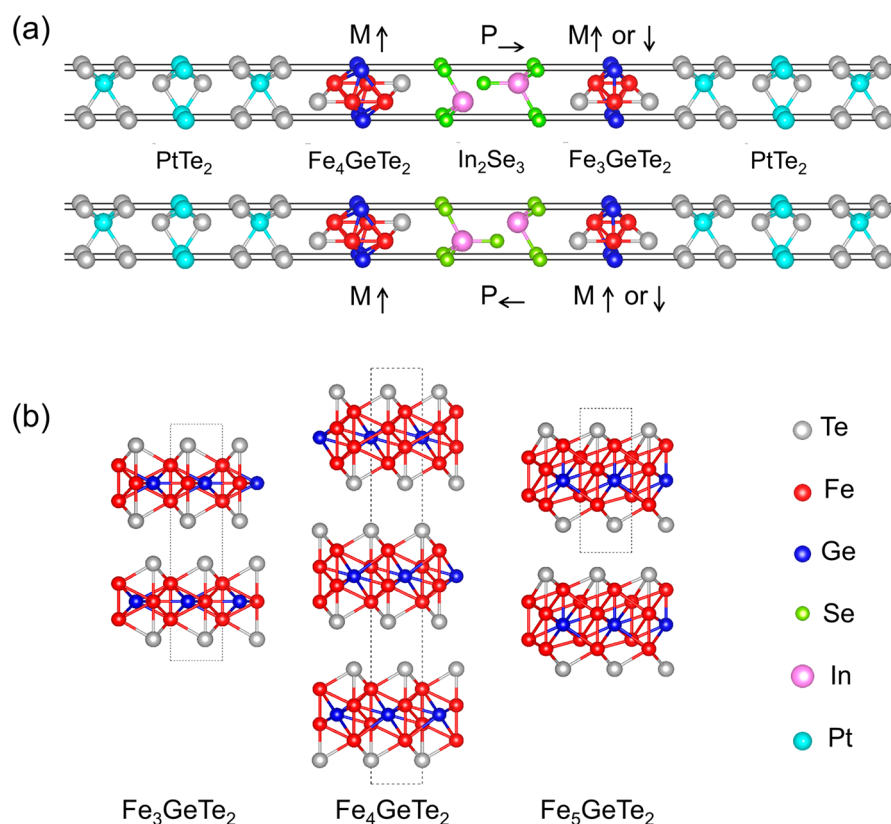


Figure 1. (a) Atomic structures of the $\text{PtTe}_2/\text{Fe}_4\text{GeTe}_2/\alpha\text{-In}_2\text{Se}_3/\text{Fe}_3\text{GeTe}_2/\text{PtTe}_2$ MFTJs. Ferroelectric polarization of In_2Se_3 is pointed right (P_{\rightarrow}) or left (P_{\leftarrow}). For the calculation of TMR, the magnetic moments of Fe atoms in Fe_4GeTe_2 are pointing up (M_{\uparrow}), while these in Fe_3GeTe_2 are pointing up (M_{\uparrow}) or down (M_{\downarrow}) for parallel or antiparallel magnetization alignment, respectively. (b) From left to right, the atomic structure of bulk Fe_3GeTe_2 , Fe_4GeTe_2 , and Fe_5GeTe_2 in a hexagonal lattice.

device application of MFTJs, can be solved using recently discovered two-dimensional (2D) van der Waals (vdW) materials.

The discovery of ferromagnetic and ferroelectric 2D vdW materials offers a new platform for exploring new physical phenomena and potential device applications.^{18,19} Heterostructures based on magnetic vdW materials have revealed novel functionalities. Specifically, it has been reported that the graphite/ CrI_3 /graphite vdW tunnel junctions exhibit a huge magnetoresistance effect over thousands of percent at low temperature.^{20–23} Among known 2D ferromagnetic vdW metals, Fe_nGeTe_2 ($n = 3, 4, 5$) compounds^{24–28} exhibit high Curie temperature T_C (about 220 K for Fe_3GeTe_2 , 280 K for Fe_4GeTe_2 , and over 300 K for Fe_5GeTe_2) and thus are promising for spintronic applications. MTJs based on these ferromagnetic vdW materials have been explored both experimentally²⁹ and theoretically.³⁰ In addition, thanks to the weak vdW interactions, the Fermi level pinning which may cause the deterioration of TMR in conventional MTJs is largely avoided in vdW MTJs.^{31,32}

In parallel with the discovery of 2D ferromagnetism, 2D ferroelectricity has been predicted and experimentally observed in vdW materials. In particular, a single layer of $\alpha\text{-In}_2\text{Se}_3$ and a similar class of $\text{III}_2\text{-VI}_3$ vdW materials have been demonstrated to exhibit 2D ferroelectricity with both in-plane and out-of-plane polarization at room temperature.^{33–36} Combining ferromagnetic and ferroelectric materials is interesting for creating functional multiferroic vdW heterostructures with magnetoelectric properties. A recent theoretical work has predicted that reversal of In_2Se_3 polarization in a $\text{Cr}_2\text{Ge}_2\text{Te}_6$ /

In_2Se_3 vdW heterostructure could change the magnetic anisotropy of $\text{Cr}_2\text{Ge}_2\text{Te}_6$.³⁷

These results point to a possibility of creating an MFTJ entirely based on the recently discovered 2D vdW ferroic materials. Because of the stable polarization of the vdW ferroelectrics, such as In_2Se_3 , down to the monolayer limit, these 2D materials can be efficiently used as ultrathin tunnel barriers in MFTJs. It is expected that in this new type of vdW MFTJs, the RA product should be much lower than that in conventional perovskite-oxide MFTJs due to the 2D ferroelectricity of the vdW barrier and its narrow energy bandgap. Thus, 2D vdW ferroic materials may provide a new and more advanced material platform for MFTJs.

In this work, using first-principles calculations based on density functional theory we investigate full vdW MFTJs and predict that they constitute reliable functional devices with multiple resistance states and a low RA product. As a representative example, we consider MFTJs composed of vdW ferromagnetic metals Fe_nGeTe_2 and a vdW ferroelectric barrier $\alpha\text{-In}_2\text{Se}_3$ and explore their spin-dependent transport properties depending on the orientation of electric polarization of In_2Se_3 and the relative magnetization alignment of Fe_nGeTe_2 . Without loss of generality, we assume that nonmagnetic metal electrodes are made of the 2H phase of PtTe_2 (2H- PtTe_2). Thus, the overall atomic structure of the considered MFTJs is $\text{PtTe}_2/\text{Fe}_m\text{GeTe}_2/\alpha\text{-In}_2\text{Se}_3/\text{Fe}_n\text{GeTe}_2/\text{PtTe}_2$. Figure 1a shows the atomic structure of the $\text{PtTe}_2/\text{Fe}_4\text{GeTe}_2/\alpha\text{-In}_2\text{Se}_3/\text{Fe}_3\text{GeTe}_2/\text{PtTe}_2$ MFTJ for the two opposite ferroelectric polarization orientations of In_2Se_3 and two magnetization alignments of Fe_4GeTe_2 and Fe_3GeTe_2 . To

calculate the transmission across the MFTJs, we proceed as follows.

The crystal structures of bulk Fe_nGeTe_2 ($n = 3, 4, 5$) are shown in Figure 1b and the experimental lattice constants of Fe_3GeTe_2 , Fe_4GeTe_2 and $\alpha\text{-In}_2\text{Se}_3$ are listed in Supporting Information (SI) Table S1. The crystal structure of bulk $\text{Fe}_{5-x}\text{GeTe}_2$ has been experimentally reported to belong either to the $R\bar{3}m$ ^{26,27} or $R3m$ ²⁸ space group. Here, for simplicity, we use the theoretically predicted crystal structure of Fe_5GeTe_2 that belongs to the $P3m1$ space group and has A-A stacking.²⁵ The in-plane lattice constants of Fe_nGeTe_2 and $\alpha\text{-In}_2\text{Se}_3$ have a mismatch of less than 1%, which allows using a (1×1) in-plane unit cell to model $\text{Fe}_m\text{GeTe}_2/\alpha\text{-In}_2\text{Se}_3/\text{Fe}_n\text{GeTe}_2$ MFTJs. The calculations are performed using Quantum ESPRESSO³⁸ within the generalized gradient approximation (GGA) for the exchange correlation potential³⁹ and the ultrasoft pseudopotential.^{40,41} A Monkhorst-Pack k -point mesh of $16 \times 16 \times 16$ and plane-wave cutoff 40 Ry are used for the self-consistent electronic structure calculations. The vdW interaction is taken into account using the DFT-D3 scheme.⁴² For the interface structures, atomic relaxations are performed using a $16 \times 16 \times 1$ Monkhorst-Pack grid for k -point sampling, and atomic positions are converged until the Hellmann–Feynman forces on each atom become less than 10^{-4} Ry/a.u. (~ 2.6 meV/Å).

First, we calculate the electronic structures of bulk Fe_nGeTe_2 and one quintuple layer (QL) thickness of In_2Se_3 . SI Figure S1 shows the calculated spin-polarized band structure and density of states (DOS) of bulk Fe_nGeTe_2 which we find consistent with the previous results.²⁵ The calculated average magnetic moment on Fe atoms is 2.10, 2.15, and 2.11 μ_B for $n = 3, 4, 5$, respectively, which are somewhat larger than the experimental values for Fe_3GeTe_2 (1.63 μ_B),²⁴ Fe_4GeTe_2 (1.8 μ_B),²⁵ and Fe_5GeTe_2 (2.0 μ_B).²⁷ This discrepancy may partly be attributed to the imperfect stoichiometry in the experimentally prepared samples.

SI Figure S2 shows the calculated band structure of 1QL and 3QL $\alpha\text{-In}_2\text{Se}_3$, indicating that 1QL $\alpha\text{-In}_2\text{Se}_3$ is a semiconductor with an indirect bandgap of 0.80 eV in agreement with the previous results (0.78 eV),³³ and the 3QL $\alpha\text{-In}_2\text{Se}_3$ is a metal with the energy bands crossing the Fermi energy. Because of the presence of a vacuum layer, the out-of-plane ferroelectric polarization of 1QL and 3QL $\alpha\text{-In}_2\text{Se}_3$ is well-defined and can be evaluated by directly integrating the charge density (see SI Section 2 for calculation details). We find that the out-of-plane electric dipole of 1QL $\alpha\text{-In}_2\text{Se}_3$ (3QL $\alpha\text{-In}_2\text{Se}_3$) is 0.092 eÅ (0.17 eÅ) and in good agreement with the previous result of 0.094 eÅ.³³ The in-plane electric dipole of 1QL $\alpha\text{-In}_2\text{Se}_3$ is calculated using the Berry phase method⁴³ to be 2.694 eÅ which is slightly larger than the value of 2.360 eÅ found in ref 33, possibly due to the smaller in-plane lattice constant of In_2Se_3 ($a = 4.026$ Å) that we have taken from experiments⁴⁴ ($a = 4.106$ Å in ref 33).

Next, we consider several possible interface atomic structures. The details of these calculations are given in SI Section 3. To build the entire atomic structure of MFTJs with the 2H-PtTe₂ electrodes, we fix the in-plane lattice constant to be 4.03 Å for PtTe₂/Fe₄GeTe₂/α-In₂Se₃/Fe₃GeTe₂/PtTe₂ and 4.026 Å for PtTe₂/Fe₅GeTe₂/α-In₂Se₃/Fe₃GeTe₂/PtTe₂ MFTJs. By performing full atomic relaxations of these MFTJs, we find the energetically favorable interface between PtTe₂ and Fe_nGeTe₂, shown in Figure 1a. Then, for each MFTJ we calculate self-consistently the electronic structure of the

supercell (such as those shown in Figure 1a) and the bulk 2H-PtTe₂ electrode. The supercell is considered as the scattering region, ideally attached on both sides to semi-infinite 2H-PtTe₂ electrodes. Next, the transport properties are calculated using the wave function scattering method⁴⁵ implemented in Quantum ESPRESSO.³⁸ The spin-dependent conductance of the tunnel junction per unit cell area is calculated as follows: $G_\sigma = \frac{e^2}{h} \sum_{\mathbf{k}_\parallel} T_\sigma(\mathbf{k}_\parallel)$, where $T_\sigma(\mathbf{k}_\parallel)$ is the transmission probability for an electron at the Fermi energy with spin σ and Bloch wave vector $\mathbf{k}_\parallel = (k_x, k_y)$, e is the elementary charge, and h is the Planck constant. In the calculations, the 2D Brillouin zone (2DBZ) is sampled using a uniform 200×200 \mathbf{k}_\parallel mesh.

We first investigate the stability of ferroelectric polarization of the 1QL $\alpha\text{-In}_2\text{Se}_3$ sandwiched between the Fe_nGeTe₂ layers. Figure 2a shows the in-plane averaged macroscopic electro-

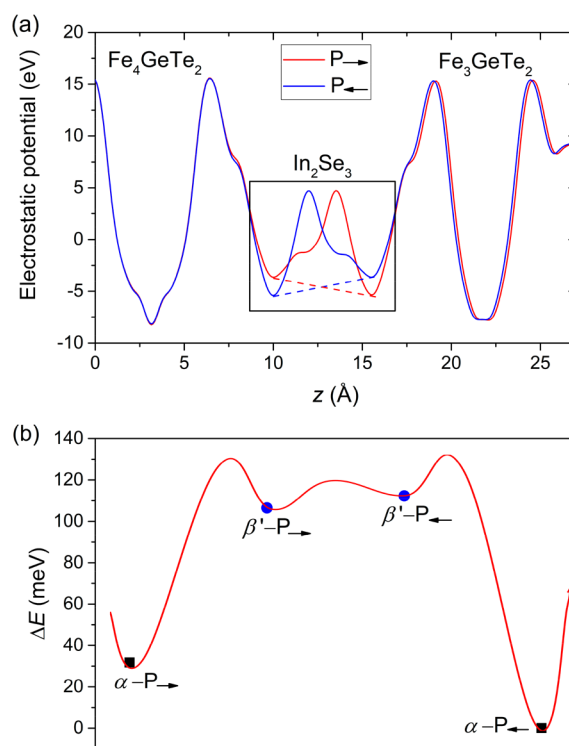


Figure 2. (a) The planar averaged macroscopic electrostatic potential in a $\text{Fe}_4\text{GeTe}_2/\alpha\text{-In}_2\text{Se}_3/\text{Fe}_3\text{GeTe}_2$ MFTJ for right (P_-) (red lines) and left (P_+) (blue lines) ferroelectric polarization. The black box indicates the region within 1QL- In_2Se_3 . The dashed lines in the black box connect the potentials between the two outmost Se layers with a slope indicating the built-in electric field induced by the electric polarization of 1QL- In_2Se_3 . (b) The total energy profile for a $\text{Fe}_4\text{GeTe}_2/1\text{QL-}\alpha\text{-In}_2\text{Se}_3/\text{Fe}_3\text{GeTe}_2$ MFTJ across ferroelectric polarization reversal of $\alpha\text{-In}_2\text{Se}_3$ involving ferroelectric states of $\beta'\text{-In}_2\text{Se}_3$.

static potential across the $\text{Fe}_4\text{GeTe}_2/\alpha\text{-In}_2\text{Se}_3/\text{Fe}_3\text{GeTe}_2$ junction for the right (P_-) and left (P_+) polarization states of In_2Se_3 . The switchable built-in electric field within the In_2Se_3 layer (dashed lines in Figure 2a) confirms the presence of ferroelectric polarization in In_2Se_3 . We find however that the net ferroelectric polarization of the whole $\text{Fe}_4\text{GeTe}_2/\alpha\text{-In}_2\text{Se}_3/\text{Fe}_3\text{GeTe}_2$ structure is reduced compared to the polarization for a free-standing 1QL $\alpha\text{-In}_2\text{Se}_3$. Specifically, for the P_- state we obtain polarization of 0.022 eÅ, which is around a quarter of the value for a free-standing $\alpha\text{-In}_2\text{Se}_3$ monolayer. This

Table 1. Calculated Spin-Dependent Electron Transmission T_{\uparrow} and T_{\downarrow} ^a

| | $M_{\uparrow\uparrow}$ (parallel magnetization) | | | | $M_{\uparrow\downarrow}$ (antiparallel magnetization) | | | | TMR |
|-------------------|---|----------------------------|---------------------------------------|-------------------------------------|---|----------------------------|---------------------------------------|-------------------------------------|------------|
| | spin up T_{\uparrow} | spin down T_{\downarrow} | $T (= T_{\uparrow} + T_{\downarrow})$ | RA ($\Omega \cdot \mu\text{m}^2$) | spin up T_{\uparrow} | spin down T_{\downarrow} | $T (= T_{\uparrow} + T_{\downarrow})$ | RA ($\Omega \cdot \mu\text{m}^2$) | |
| P_{\rightarrow} | 1.48×10^{-2} | 7.11×10^{-3} | 2.19×10^{-2} | 0.17 | 5.82×10^{-3} | 5.76×10^{-3} | 1.16×10^{-2} | 0.31 | 89% |
| P_{\leftarrow} | 2.29×10^{-2} | 7.85×10^{-3} | 3.08×10^{-2} | 0.12 | 4.40×10^{-3} | 1.44×10^{-2} | 1.88×10^{-2} | 0.19 | 64% |
| TER | 41% | | | | 62% | | | | |

^aAlso the RA product, the TMR (in bold) for left and right polarizations of the In_2Se_3 barrier layer and the TER (in bold) for parallel and antiparallel magnetization alignments of the two ferromagnetic Fe_nGeTe_2 layers in the $\text{PtTe}_2/\text{Fe}_4\text{GeTe}_2/\alpha\text{-In}_2\text{Se}_3/\text{Fe}_3\text{GeTe}_2/\text{PtTe}_2$ MFTJ.

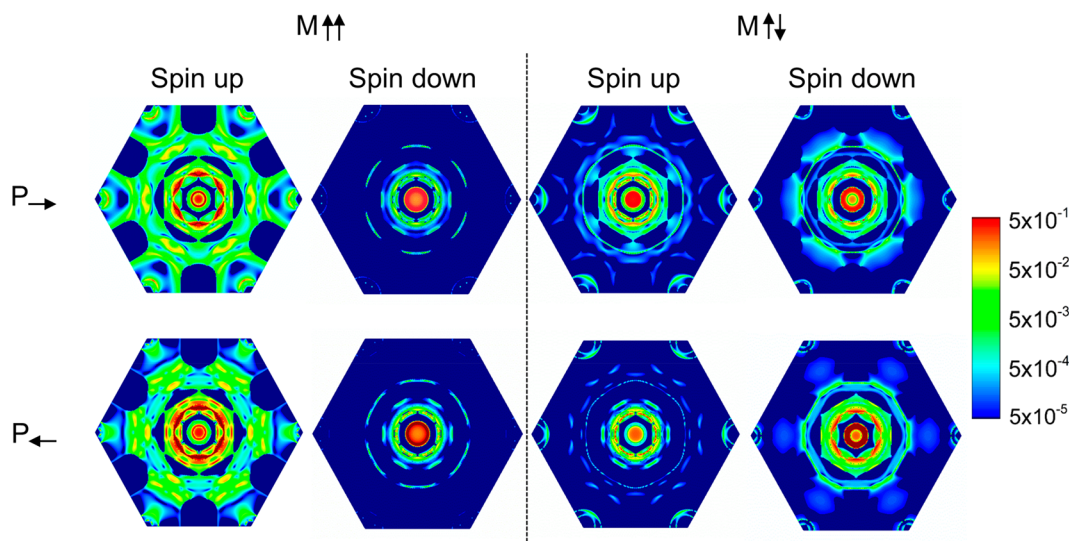


Figure 3. Electron transmission for spin-up and spin-down conduction channels in 2DBZ for $\text{PtTe}_2/\text{Fe}_4\text{GeTe}_2/\alpha\text{-In}_2\text{Se}_3/\text{Fe}_3\text{GeTe}_2/\text{PtTe}_2$ MFTJ with right (P_{\rightarrow}) and left (P_{\leftarrow}) ferroelectric polarizations of In_2Se_3 and parallel ($M_{\uparrow\uparrow}$) and antiparallel ($M_{\uparrow\downarrow}$) magnetization alignments of Fe_4GeTe_2 and Fe_3GeTe_2 . The transmission intensity is indicated in logarithmic scale by different colors.

reduction of the ferroelectric polarization can be attributed to the charge transfer between Fe_nGeTe_2 and In_2Se_3 .⁴⁶

An important point to address is the stability of the ferroelectric state of $\alpha\text{-In}_2\text{Se}_3$ in the $\text{Fe}_4\text{GeTe}_2/\alpha\text{-In}_2\text{Se}_3/\text{Fe}_3\text{GeTe}_2$ structure against transition to the $\beta'\text{-In}_2\text{Se}_3$ phase. We calculate the total energy of the $\text{Fe}_4\text{GeTe}_2/1\text{QL-In}_2\text{Se}_3/\text{Fe}_3\text{GeTe}_2$ heterostructure across the ferroelectric phase transition involving both the α and β' phases of In_2Se_3 . The results shown in Figure 2 demonstrate that both polarization states of $\alpha\text{-In}_2\text{Se}_3$ have a lower total energy compared to the $\beta'\text{-In}_2\text{Se}_3$ phase, which confirms the bistable ferroelectric state of $\alpha\text{-In}_2\text{Se}_3$ in the sandwiched structure.

The calculated transport properties of the $\text{PtTe}_2/\text{Fe}_4\text{GeTe}_2/\alpha\text{-In}_2\text{Se}_3/\text{Fe}_3\text{GeTe}_2/\text{PtTe}_2$ MFTJ are shown in Table 1. The TMR ratio is defined as $\text{TMR} = (G_{\text{P}} - G_{\text{AP}})/G_{\text{AP}}$, where G_{P} and G_{AP} are the conductances for parallel ($M_{\uparrow\uparrow}$) and antiparallel ($M_{\uparrow\downarrow}$) magnetization alignments of the two ferromagnetic Fe_nGeTe_2 layers, respectively. Similarly, the TER ratio is defined as $\text{TER} = (G_{\text{L}} - G_{\text{R}})/G_{\text{R}}$, where G_{R} and G_{L} are the conductances for right (P_{\rightarrow}) and left (P_{\leftarrow}) polarization directions of the ferroelectric In_2Se_3 layers, respectively. As is evident from Table 1, the TMR depends on ferroelectric polarization of In_2Se_3 and is calculated to be 89% and 64%, for right and left polarization orientations, respectively. The TMR originates from the dissimilar electronic structures for majority and minority spins of Fe_nGeTe_2 which are evident from the exchange split electronic structures shown in SI Figure S1 as well as the spin-dependent Fermi surfaces shown in SI Figure S6.

The presence of different ferromagnetic layers, that is, Fe_4GeTe_2 and Fe_3GeTe_2 , terminating the semi-infinite PtTe_2 electrodes produce asymmetry in the MFTJ which is necessary for the nonzero TER effect.⁸ We find that the TER ratio is 41% and 62% for parallel and antiparallel magnetization alignment of ferromagnetic layers, respectively (Table 1). These values are not as large as those in some perovskite-oxide FTJs,^{10,11} which is explained by the small out-of-plane polarization and the similar atomic and electronic structures of the left and right Fe_nGeTe_2 interfaces in the MFTJs.

We find that the ferroelectric polarization reversal of In_2Se_3 mainly changes the transmission of the spin-up electrons for parallel magnetization and spin-down electrons for antiparallel magnetization of the ferromagnetic Fe_4GeTe_2 and Fe_3GeTe_2 layers from Table 1. Noting that the spin-up and spin-down notation is referred to the electron spin in Fe_4GeTe_2 , this fact indicates that the polarization switching mostly affects the spin-up transmission of Fe_3GeTe_2 . This can be understood by looking at changes in the interface atomic structure upon ferroelectric polarization switching. Specifically, the interface distance between Fe_3GeTe_2 and $\alpha\text{-In}_2\text{Se}_3$ is 0.170 \AA for the P_{\leftarrow} state which is smaller than that for the P_{\rightarrow} state (Figure S5). This produces a larger transmission across the interface between the Fe_3GeTe_2 and $\alpha\text{-In}_2\text{Se}_3$ layers for the P_{\leftarrow} polarization especially in the spin-up conduction channel, as we will discuss later.

Overall, as seen from Table 1, the electron transmission and the associated RA product (see details for the RA calculation in SI Section 5) reveal four resistance states of the $\text{PtTe}_2/\text{Fe}_4\text{GeTe}_2/\alpha\text{-In}_2\text{Se}_3/\text{Fe}_3\text{GeTe}_2/\text{PtTe}_2$ MFTJ. These states are

distinguished by the different magnetic alignments of the ferromagnetic Fe_nGeTe_2 layers and different polarization directions of the ferroelectric In_2Se_3 layer. It is important to point out that the calculated RA products for all four resistance states are less than $1 \Omega \cdot \mu\text{m}^2$ which is a desirable feature of an MFTJ for device applications. This is in contrast to the previously calculated RA products for perovskite-oxide MFTJs of around several $k\Omega \cdot \mu\text{m}^2$.^{10,11} We observe similar features of TMR, TER, and RA products for a $\text{PtTe}_2/\text{Fe}_5\text{GeTe}_2/\alpha\text{-In}_2\text{Se}_3/\text{Fe}_3\text{GeTe}_2/\text{PtTe}_2$ MFTJ (see Table S2 in SI).

Such low RA products in the proposed MFTJ can be attributed to the small bandgap of $\alpha\text{-In}_2\text{Se}_3$. Figure S8 shows the atomic weight projected band structures of the $\text{Fe}_4\text{GeTe}_2/\alpha\text{-In}_2\text{Se}_3/\text{Fe}_3\text{GeTe}_2$ MFTJ for ferroelectric polarization pointing right and left. The valence band maximum (VBM) of 1QL $\alpha\text{-In}_2\text{Se}_3$ is found to be 1.14 eV below the Fermi energy due to the band alignment between Fe_nGeTe_2 and In_2Se_3 . As a result, the Fermi energy crosses the conduction bands of $\alpha\text{-In}_2\text{Se}_3$ and leads to the small RA.

Increasing $\alpha\text{-In}_2\text{Se}_3$ thickness above 1 QL makes it metallic.³³ Figure S2b shows the calculated band structure and DOS of 3QL $\alpha\text{-In}_2\text{Se}_3$ which demonstrate that several energy bands cross the Fermi energy. Table S3 shows the results of transport calculations for a $\text{PtTe}_2/\text{Fe}_4\text{GeTe}_2/\alpha\text{-In}_2\text{Se}_3$ (3QL)/ $\text{Fe}_3\text{GeTe}_2/\text{PtTe}_2$ MFTJ where 3QL $\alpha\text{-In}_2\text{Se}_3$ is used as a spacer layer. We find that both TMR and TER are around tens of a percent and the RAs are lower than $1 \Omega \cdot \mu\text{m}^2$ which prove the robustness of the MFTJ regardless of the barrier layer thickness and the conduction type of the $\alpha\text{-In}_2\text{Se}_3$ film.

To elucidate in more detail the effects of ferroelectric polarization and magnetization alignment on electron transmission, we calculate the \mathbf{k}_{\parallel} - and spin-resolved transmission $T_{\sigma}(\mathbf{k}_{\parallel})$ of $\text{PtTe}_2/\text{Fe}_4\text{GeTe}_2/\alpha\text{-In}_2\text{Se}_3/\text{Fe}_3\text{GeTe}_2/\text{PtTe}_2$ MFTJ in the 2DBZ. The results are shown in Figure 3 for parallel ($M_{\uparrow\uparrow}$) and antiparallel ($M_{\uparrow\downarrow}$) magnetization alignments of the Fe_4GeTe_2 and Fe_3GeTe_2 layers with right (P_{\rightarrow}) and left (P_{\leftarrow}) ferroelectric polarizations of In_2Se_3 . The overall transmission patterns reflect the distribution of the available conduction channels of the 2D Fermi surface of the 2H- PtTe_2 electrodes displayed in SI Figure S7. There is a relatively large transmission around the $\bar{\Gamma}$ point ($\mathbf{k}_{\parallel} = 0$) of the 2DBZ. It is clearly seen that the transmission of the MFTJ is modulated by reversing the ferroelectric polarization of In_2Se_3 . In particular, when the ferroelectric polarization is pointing left (P_{\leftarrow}), transmission of the spin-up channel for parallel ($M_{\uparrow\uparrow}$) magnetization and transmission of the spin-down channel for antiparallel ($M_{\uparrow\downarrow}$) magnetization are large. That is, the left polarization (P_{\leftarrow}) enhances the transmission of the spin-up channel in Fe_3GeTe_2 layer.

This behavior can be understood as follows. The transmission for an electron with spin σ across a junction can be approximated by the following expression^{10,47}

$$T_{\sigma}(\mathbf{k}_{\parallel}) = t_L^{\sigma}(\mathbf{k}_{\parallel})t_C^{\sigma}(\mathbf{k}_{\parallel})t_R^{\sigma}(\mathbf{k}_{\parallel})$$

where $t_L^{\sigma}(\mathbf{k}_{\parallel})$ and $t_R^{\sigma}(\mathbf{k}_{\parallel})$ are the interface transmission functions at left ($\text{Fe}_4\text{GeTe}_2/\alpha\text{-In}_2\text{Se}_3$) and right ($\text{Fe}_3\text{GeTe}_2/\alpha\text{-In}_2\text{Se}_3$) interfaces, respectively, and $t_C^{\sigma}(\mathbf{k}_{\parallel})$ is the transmission function across the In_2Se_3 layer. As we discussed previously, for the left (P_{\leftarrow}) ferroelectric polarization, the $\text{Fe}_3\text{GeTe}_2/\alpha\text{-In}_2\text{Se}_3$ interface distance is smaller, and therefore transmission $t_R^{\sigma}(\mathbf{k}_{\parallel})$ is larger. The stronger interface hybridization for the spin-up electrons with the left (P_{\leftarrow}) ferroelectric

polarization can also be seen from the projected band structure shown in Figure S8.

To demonstrate that the multiple resistance states are robust against the electronic structure of the electrodes, we calculate RA products for $\text{PtTe}_2/\text{Fe}_4\text{GeTe}_2/\text{In}_2\text{Se}_3/\text{Fe}_3\text{GeTe}_2/\text{PtTe}_2$ and $\text{PtTe}_2/\text{Fe}_5\text{GeTe}_2/\text{In}_2\text{Se}_3/\text{Fe}_3\text{GeTe}_2/\text{PtTe}_2$ MFTJs by varying the position of the Fermi energy within the range of $E_F \pm 0.1$ eV. The calculated RA products for different polarization and magnetization orientations are shown in Figure 4. One can see that for different Fermi energies, the

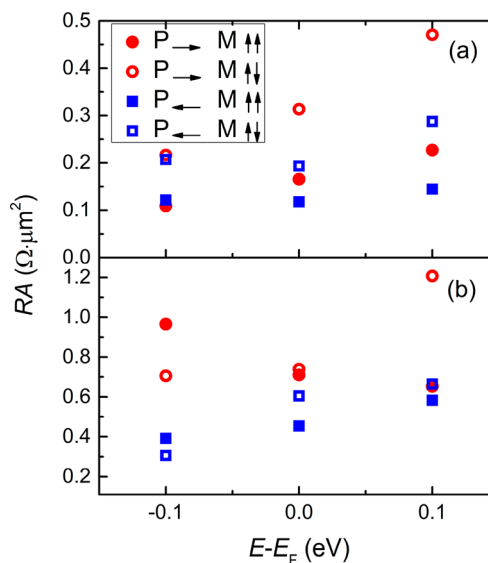


Figure 4. RA products of the multiple resistance states as a function of the Fermi energy ranging from $E_F - 0.1$ eV to $E_F + 0.1$ eV for (a) $\text{PtTe}_2/\text{Fe}_4\text{GeTe}_2/\alpha\text{-In}_2\text{Se}_3/\text{Fe}_3\text{GeTe}_2/\text{PtTe}_2$ and (b) $\text{PtTe}_2/\text{Fe}_5\text{GeTe}_2/\alpha\text{-In}_2\text{Se}_3/\text{Fe}_3\text{GeTe}_2/\text{PtTe}_2$ MFTJs. The data shown in red circles and blue squares correspond to the right (P_{\rightarrow}) and left (P_{\leftarrow}) ferroelectric polarizations of $\alpha\text{-In}_2\text{Se}_3$, respectively. The data shown in solid and hollow symbols correspond to the parallel ($M_{\uparrow\uparrow}$) and antiparallel ($M_{\uparrow\downarrow}$) magnetization alignments of the Fe_nGeTe_2 layers, respectively.

multiple resistance states are preserved. However, the particular RA values of the four resistance states depend on the Fermi energy. For instance, for $\text{PtTe}_2/\text{Fe}_4\text{GeTe}_2/\text{In}_2\text{Se}_3/\text{Fe}_3\text{GeTe}_2/\text{PtTe}_2$ MFTJ, the multiple resistance states are more separated for $E = E_F$ and $E = E_F + 0.1$ eV, while for $\text{PtTe}_2/\text{Fe}_5\text{GeTe}_2/\text{In}_2\text{Se}_3/\text{Fe}_3\text{GeTe}_2/\text{PtTe}_2$ MFTJ, the multiple resistance states are more separated at $E = E_F - 0.1$ eV. The absolute difference of RA does rely on the position of the Fermi energy since at different energies the electronic structures of the electrode, ferromagnetic layers and the barrier are all altered.

The proposed MFTJs are feasible for experimental fabrication. Parallel ($M_{\uparrow\uparrow}$) and antiparallel ($M_{\uparrow\downarrow}$) magnetization alignments of Fe_nGeTe_2 can be realized thanks to their different coercivities⁶ and a weak interlayer exchange coupling (IEC) of two Fe_nGeTe_2 layers through In_2Se_3 (see Section 7 of SI). In_2Se_3 and similar III₂-VI₃ vdW ferroelectric materials possess both in-plane and out-of-plane polarizations. That polarization switching can be realized by applying the electric field either in-plane or out-of-plane.³⁶ Experimentally, out-of-plane (in-plane) switching of In_2Se_3 has been achieved in an electric field of 200 kV/cm (40 kV/cm).⁴⁸ Therefore, the nonvolatile multiple states with switchable ferroelectric polar-

izations of In_2Se_3 and magnetization alignments of Fe_nGeTe_2 can be realized.

The stability of ferroelectric polarization of In_2Se_3 QDs sandwiched between magnetic vdW metal layers is an important advantage of vdW ferroelectrics. The low RA in the proposed MFTJs stems from the small bandgap of 1QL- In_2Se_3 and its conduction bands align with the Fermi level of Fe_nGeTe_2 , or from the metallic feature when the thickness of In_2Se_3 is larger than 2QLs. The TMR and TER in the proposed vdW MFTJs are around tens of a percent and can be further enhanced by using appropriate materials. For instance, TMR can be enhanced by using thicker Fe_nGeTe_2 layers which are expected to recover the spin-polarized bulk band structure.⁴⁹ A larger TER can be achieved by exploiting vdW materials with a moderate out-of-plane polarization, or by asymmetric interface engineering. A few examples of this approach are reported in Section 8 of SI.

In summary, we have introduced a concept of the vdW MFTJ, which may serve as a feasible analog of the perovskite-oxide MFTJ but could produce a better performance for device applications due to their scalability down to the nanometer layer thickness and a low RA product. As an example, we have considered vdW MFTJ consisting of Fe_nGeTe_2 ferromagnetic electrodes and In_2Se_3 tunnel barriers. Using first-principles calculations based on density functional theory, we have predicted the presence of four resistance states in these vdW MFTJs and an ultralow RA product. We hope that our theoretical predictions will stimulate experimental efforts to explore new functionalities of the proposed vdW MFTJs.

■ ASSOCIATED CONTENT

SI Supporting Information

The Supporting Information is available free of charge at <https://pubs.acs.org/doi/10.1021/acs.nanolett.0c03452>.

Atomic and electronic structure of bulk Fe_nGeTe_2 ($n = 3, 4, 5$); atomic and electronic structure of $\alpha\text{-In}_2\text{Se}_3$; the calculation of the out-of-plane ferroelectric polarization for 1QL and 3QL $\alpha\text{-In}_2\text{Se}_3$; interface atomic structure of $\text{Fe}_n\text{GeTe}_2/\alpha\text{-In}_2\text{Se}_3/\text{Fe}_3\text{GeTe}_2$; electronic structure of the $\text{PtTe}_2/\text{Fe}_n\text{GeTe}_2/\alpha\text{-In}_2\text{Se}_3/\text{Fe}_3\text{GeTe}_2/\text{PtTe}_2$ MFTJ; calculation of the RA product; calculated transport properties of the $\text{PtTe}_2/\text{Fe}_3\text{GeTe}_2/\alpha\text{-In}_2\text{Se}_3$ (1QL)/ $\text{Fe}_3\text{GeTe}_2/\text{PtTe}_2$ and the $\text{PtTe}_2/\text{Fe}_4\text{GeTe}_2/\alpha\text{-In}_2\text{Se}_3$ (3QL)/ $\text{Fe}_3\text{GeTe}_2/\text{PtTe}_2$ MFTJs; interlayer exchange coupling of Fe_nGeTe_2 through 1QL $\alpha\text{-In}_2\text{Se}_3$; transport in MFTJs with thicker Fe_nGeTe_2 layers and vdW magnet Co_4GeTe_2 (PDF)

■ AUTHOR INFORMATION

Corresponding Authors

Jia Zhang – School of Physics and Wuhan National High Magnetic Field Center, Huazhong University of Science and Technology, 430074 Wuhan, China; orcid.org/0000-0002-4125-2269; Email: jiazhang@hust.edu.cn

Long You – School of Optical and Electronic Information, Huazhong University of Science and Technology, 430074 Wuhan, China; orcid.org/0000-0001-5713-194X; Email: lyou@hust.edu.cn

Evgeny Y. Tsybmal – Department of Physics and Astronomy and Nebraska Center for Materials and Nanoscience, University of Nebraska, Lincoln, Nebraska 68588, United

States; orcid.org/0000-0002-6728-5480;

Email: tsybmal@unl.edu

Authors

Yurong Su – School of Optical and Electronic Information, Huazhong University of Science and Technology, 430074 Wuhan, China; orcid.org/0000-0003-2237-9771

Xinlu Li – School of Physics and Wuhan National High Magnetic Field Center, Huazhong University of Science and Technology, 430074 Wuhan, China

Meng Zhu – School of Physics and Wuhan National High Magnetic Field Center, Huazhong University of Science and Technology, 430074 Wuhan, China

Complete contact information is available at:

<https://pubs.acs.org/doi/10.1021/acs.nanolett.0c03452>

Notes

The authors declare no competing financial interest.

■ ACKNOWLEDGMENTS

L.Y. and J.Z. acknowledge support from the National Natural Science Foundation of China (Grants 11704135, 61674062, and 61821003). Computations were partly performed by utilizing TianHe-2 at the National Supercomputer Center in Guangzhou, China, and the Platform for Data-Driven Computational Materials Discovery at the Songshan Lake Materials Laboratory, Dongguan, China. The authors thank Prof. Jun Sung Kim from Department of Physics, Pohang University of Science and Technology, Korea for providing the structural parameters of bulk Fe_4GeTe_2 and Fe_5GeTe_2 and Dr. X. K. Huang from Jingdezhen Ceramic Institute, China for helpful discussions.

■ REFERENCES

- (1) Jullière, M. Tunneling between ferromagnetic films. *Phys. Lett. A* **1975**, *54*, 225–226.
- (2) Tsybmal, E.; Y. Mryasov, O. N.; LeClair, P. R. Spin-dependent tunnelling in magnetic tunnel junctions. *J. Phys.: Condens. Matter* **2003**, *15*, R109–R142.
- (3) Tsybmal, E. Y.; Kohlstedt, H. Tunneling across a ferroelectric. *Science* **2006**, *313*, 181–183.
- (4) Zhuravlev, M. Y.; Sabirianov, R. F.; Jaswal, S. S.; Tsybmal, E. Y. Giant electroresistance in ferroelectric tunnel junctions. *Phys. Rev. Lett.* **2005**, *94*, 246802.
- (5) Kohlstedt, H.; Pertsev, N. A.; Contreras, J. R.; Waser, R. Theoretical current-voltage characteristics of ferroelectric tunnel junctions. *Phys. Rev. B: Condens. Matter Mater. Phys.* **2005**, *72*, 125341.
- (6) Zhuravlev, M. Y.; Maekawa, S.; Tsybmal, E. Y. Effect of spin-dependent screening on tunneling electroresistance and tunneling magnetoresistance in multiferroic tunnel junctions. *Phys. Rev. B: Condens. Matter Mater. Phys.* **2010**, *81*, 104419.
- (7) Garcia, V.; Bibes, M. Ferroelectric tunnel junctions for information storage and processing. *Nat. Commun.* **2014**, *5*, 4289.
- (8) Velev, J. P.; Burton, J. D.; Zhuravlev, M. Y.; Tsybmal, E. Y. Predictive modelling of ferroelectric tunnel junctions. *npj Comput. Mater.* **2016**, *2*, 16009.
- (9) Wen, Z.; Wu, D. Ferroelectric Tunnel Junctions: Modulations on the Potential Barrier. *Adv. Mater.* **2019**, *27*, 1904123.
- (10) Velev, J. P.; Duan, C.; Burton, J. D.; Smogunov, A.; Niranjan, M. K.; Tosatti, E.; Jaswal, S. S.; Tsybmal, E. Y. Magnetic tunnel junctions with ferroelectric barriers: Prediction of four resistance states from first principles. *Nano Lett.* **2009**, *9*, 427–432.
- (11) Borisov, V. S.; Ostanin, S.; Achilles, S.; Henk, J.; Mertig, I. Spin-dependent transport in a multiferroic tunnel junction: Theory for Co/

PbTiO₃/Co. *Phys. Rev. B: Condens. Matter Mater. Phys.* **2015**, *92*, No. 075137.

(12) Garcia, V.; et al. Ferroelectric control of spin polarization. *Science* **2010**, *327*, 1106–1110.

(13) Hambe, M.; Petraru, A.; Pertsev, N. A.; Munroe, P.; Nagarajan, V.; Kohlstedt, H. Crossing an interface: Ferroelectric control of tunnel currents in magnetic complex oxide heterostructures. *Adv. Funct. Mater.* **2010**, *20*, 2436–2441.

(14) Valencia, S.; et al. Interface-induced room-temperature multiferroicity in BaTiO₃. *Nat. Mater.* **2011**, *10*, 753.

(15) Pantel, D.; Goetze, S.; Hesse, D.; Alexe, M. Reversible electrical switching of spin polarization in multiferroic tunnel junctions. *Nat. Mater.* **2012**, *11*, 289–293.

(16) Nagamine, Y.; Maehara, H.; Tsunekawa, K.; Djayaprawira, D. D.; Watanabe, N.; Yuasa, S.; Ando, K. Ultralow resistance-area product of 0.4 Ω(μm)² and high magnetoresistance above 50% in CoFeB/MgO/CoFeB magnetic tunnel junctions. *Appl. Phys. Lett.* **2006**, *89*, 162507.

(17) Yakushiji, K.; Noma, K.; Saruya, T.; Kubota, H.; Fukushima, A.; Nagahama, T.; Yuasa, S.; Ando, K. High Magnetoresistance Ratio and Low Resistance–Area Product in Magnetic Tunnel Junctions with Perpendicularly Magnetized Electrodes. *Appl. Phys. Express* **2010**, *3*, No. 053003.

(18) Burch, K. S.; Mandrus, D.; Park, J.-G. Magnetism in two-dimensional van der Waals materials. *Nature* **2018**, *563*, 47–52.

(19) Gong, C.; Zhang, X. Two-dimensional magnetic crystals and emergent heterostructure devices. *Science* **2019**, *363*, No. eaav4450.

(20) Song, T.; et al. Giant tunneling magnetoresistance in spin-filter van der Waals heterostructures. *Science* **2018**, *360*, 1214–1218.

(21) Klein, D. R.; et al. Probing magnetism in 2D van der Waals crystalline insulators via electron tunneling. *Science* **2018**, *360*, 1218–1222.

(22) Wang, Z.; Gutiérrez-Lezama, I.; Ubrig, N.; Kroner, M.; Gibertini, M.; Taniguchi, T.; Watanabe, K.; Imamoğlu, A.; Giannini, E.; Morpurgo, A. F. Very large tunneling magnetoresistance in layered magnetic semiconductor CrI₃. *Nat. Commun.* **2018**, *9*, 2516.

(23) Paudel, T. R.; Tsymbal, E. Y. Spin filtering in CrI₃ tunnel junctions. *ACS Appl. Mater. Interfaces* **2019**, *11*, 15781–15787.

(24) Chen, B.; Yang, J.; Wang, H.; Imai, M.; Ohta, H.; Michioka, C.; Yoshimura, K.; Fang, M. Magnetic properties of layered itinerant electron ferromagnet Fe₃GeTe₂. *J. Phys. Soc. Jpn.* **2013**, *82*, 124711.

(25) Seo, J.; et al. Nearly room temperature ferromagnetism in a magnetic metal-rich van der Waals metal. *Sci. Adv.* **2020**, *6*, No. eaay8912.

(26) May, A. F.; Ovchinnikov, D.; Zheng, Q.; Hermann, R. P.; Calder, S.; Huang, B.; Fei, Z.; Liu, Y.; Xu, X.; McGuire, M. A. Ferromagnetism near room temperature in the cleavable van der Waals crystal Fe₃GeTe₂. *ACS Nano* **2019**, *13*, 4436–4442.

(27) May, A. F.; Bridges, C. A.; McGuire, M. A. Physical properties and thermal stability of Fe_{5-x}GeTe₂ single crystals. *Phys. Rev. Materials* **2019**, *3*, 104401.

(28) Stahl, J.; Shlaen, E.; Johrendt, D. The van der Waals Ferromagnets Fe_{5-δ}GeTe₂ and Fe_{5-δ-x}Ni_xGeTe₂—Crystal Structure, Stacking Faults, and Magnetic Properties. *Z. Anorg. Allg. Chem.* **2018**, *644*, 1923.

(29) Wang, Z.; Sapkota, D.; Taniguchi, T.; Watanabe, K.; Mandrus, D.; Morpurgo, A. F. Tunneling spin valves based on Fe₃GeTe₂/hBN/Fe₃GeTe₂ van der Waals Heterostructures. *Nano Lett.* **2018**, *18*, 4303–4308.

(30) Li, X.; Lü, J.; Zhang, J.; You, L.; Su, Y.; Tsymbal, E. Y. Spin-dependent transport in van der Waals magnetic tunnel junctions with Fe₃GeTe₂ electrodes. *Nano Lett.* **2019**, *19*, 5133–5139.

(31) Liu, Y.; Stradins, P.; Wei, S.-H. Van der Waals metal-semiconductor junction: Weak Fermi level pinning enables effective tuning of Schottky barrier. *Sci. Adv.* **2016**, *2*, No. e1600069.

(32) Roy, M. A.; Nikonov, D. E.; Young, I. A. Atomistic simulation of tunneling magnetoresistance using extended Hückel theory. *J. Appl. Phys.* **2012**, *112*, 104510.

(33) Ding, W.; Zhu, J.; Wang, Z.; Gao, Y.; Xiao, D.; Gu, Y.; Zhang, Z.; Zhu, W. Prediction of intrinsic two-dimensional ferroelectrics in In₂Se₃ and other III₂-VI₃ van der Waals materials. *Nat. Commun.* **2017**, *8*, 14956.

(34) Zhou, Y.; et al. Out-of-plane piezoelectricity and ferroelectricity in layered α-In₂Se₃ nanoflakes. *Nano Lett.* **2017**, *17*, 5508–5513.

(35) Cui, C.; et al. Intercorrelated in-plane and out-of-plane ferroelectricity in ultrathin two-dimensional layered semiconductor In₂Se₃. *Nano Lett.* **2018**, *18*, 1253–1258.

(36) Xiao, J.; et al. Intrinsic two-dimensional ferroelectricity with dipole locking. *Phys. Rev. Lett.* **2018**, *120*, 227601.

(37) Gong, C.; Kim, E. M.; Wang, Y.; Lee, G.; Zhang, X. Multiferroicity in atomic van der Waals heterostructures. *Nat. Commun.* **2019**, *10*, 2657.

(38) Giannozzi, P.; et al. Advanced capabilities for materials modelling with Quantum ESPRESSO. *J. Phys.: Condens. Mater.* **2017**, *29*, 465901.

(39) Perdew, J. P.; Burke, K.; Ernzerhof, M. Generalized gradient approximation made simple. *Phys. Rev. Lett.* **1996**, *77*, 3865–3868.

(40) Vanderbilt, D. Soft self-consistent pseudopotentials in a generalized eigenvalue formalism. *Phys. Rev. B: Condens. Matter Mater. Phys.* **1990**, *41*, 7892–7895.

(41) Garrity, K. F.; Bennett, J. W.; Rabe, K. M.; Vanderbilt, D. Pseudopotentials for high-throughput DFT calculations. *Comput. Mater. Sci.* **2014**, *81*, 446–452.

(42) Grimme, S.; Antony, J.; Ehrlich, S.; Krieg, H. A consistent and accurate ab initio parametrization of density functional dispersion correction (DFT-D) for the 94 elements H-Pu. *J. Chem. Phys.* **2010**, *132*, 154104.

(43) Kingsmith, R. D.; Vanderbilt, D. Theory of polarization of crystalline solids. *Phys. Rev. B: Condens. Matter Mater. Phys.* **1993**, *47*, 1651–1654.

(44) KüPers, M.; Konze, P. M.; Meledin, A.; Mayer, J.; Englert, U.; Wuttig, M.; Dronskowski, R. Controlled crystal growth of indium selenide, In₂Se₃, and the crystal structures of α-In₂Se₃. *Inorg. Chem.* **2018**, *57*, 11775–11781.

(45) Smogunov, A.; Corso, A. D.; Tosatti, E. Ballistic conductance of magnetic Co and Ni nanowires with ultrasoft pseudopotentials. *Phys. Rev. B: Condens. Matter Mater. Phys.* **2004**, *70*, No. 045417.

(46) Huang, X.; Li, G.; Chen, C.; Nie, X.; Jiang, X.; Liu, J. Interfacial coupling induced critical thickness for the ferroelectric bistability of two-dimensional ferromagnet/ferroelectric van der Waals heterostructures. *Phys. Rev. B: Condens. Matter Mater. Phys.* **2019**, *100*, 235445.

(47) Belashchenko, K. D.; Tsymbal, E. Y.; van Schilfgaarde, M.; Stewart, D. A.; Oleynik, I. I.; Jaswal, S. S. Effect of interface bonding on spin-dependent tunneling from the oxidized Co surface. *Phys. Rev. B: Condens. Matter Mater. Phys.* **2004**, *69*, 174408.

(48) Li, Y.; Chen, C.; Li, W.; Mao, X.; Liu, H.; Xiang, J.; Nie, A.; Liu, Z.; Zhu, W.; Zeng, H. Orthogonal electric control of the out-of-plane field-effect in 2D ferroelectric α-In₂Se₃. *Adv. Electron. Mater.* **2020**, *6*, 2000061.

(49) Heiliger, C.; Gradhand, M.; Zahn, P.; Mertig, I. Tunneling magnetoresistance on the subnanometer scale. *Phys. Rev. Lett.* **2007**, *99*, No. 066804.